Opto-Electronic Advances

Supplementary information

May 2023, Vol. 6, No. 5

DOI: 10.29026/oea.2023.220061

Janus aramid nanofiber aerogel incorporating plasmonic nanoparticles for high-efficiency interfacial solar steam generation

Hui Zhang[1,2†], Lei Feng[1,2†], Fengyue Wang[1], Mingze Liu[1], Yingying Zhang[1], Jia Zhu[1,2], Yanqing Lu[1,2] and Ting Xu[1,2*]

[1]National Laboratory of Solid-State Microstructures, Jiangsu Key Laboratory of Artificial Functional Materials, College of Engineering and Applied Sciences, Nanjing University, Nanjing 210093, China; [2]Collaborative Innovation Center of Advanced Microstructures, Nanjing 210093, China.
[†]These authors contributed equally to this work.
*Correspondence: T Xu, Email: xuting@nju.edu.cn

This file includes:

Supplementary information for this paper is available at https://doi.org/10.29026/oea.2023.220061

Open Access This article is licensed under a Creative Commons Attribution 4.0 International License.
To view a copy of this license, visit http://creativecommons.org/licenses/by/4.0/.

© The Author(s) 2023. Published by Institute of Optics and Electronics, Chinese Academy of Sciences.

Section 1: Chemical structure of Janus aramid nanofiber aerogel (JANA)

To interpret the chemical composition of JANA, we measured the IR absorption by using FTIR spectroscopy. Figure S1(a) demonstrates the molecular structure of conventional aramid. Characteristic functional groups include carboxyl groups, imino groups, and benzene rings. Figure S1(b) is the FT-IR spectrum of aramid nanofiber aerogel (ANA), which is highly similar to functionalized aramid[S1]. The 3300 $cm^{-1}$and 1540 cm^{-1} peaks respectively feature the stretching and bending frequencies of N-H bonds; 1650 cm^{-1} peak features the C=O and C=N stretches; 1515 cm^{-1}, 1406 cm^{-1}, and 864 cm^{-1} peaks are generated from the benzene rings. The splitting and broadening of the N-H and C=O stretching peaks are caused by the phosphoric acid hydrolysis and glutaraldehyde condensation reactions. The 2845 cm^{-1} peak features the alkyl chains from glutaraldehyde. Figure S1(c) is the FT-IR spectrum of plasmonic aramid nanofiber aerogel (PANA), which is ANA combined with Au nanoparticles. All the peaks generated from C=O, N-H, and benzene rings are slightly shifted, but the ones generated from alkyl chains remain nearly the same. This is caused by the formation of hydrogen bonds between the oxygen/nitrogen atoms of ANA and the carboxylic acid groups of the citrates coating the Au nanoparticles. Accordingly, the chemical variation from conventional aramid to JANA is a result of comprehensive reactions including phosphoric acid hydrolysis, glutaraldehyde condensation, and citrate hydrogen bonding.

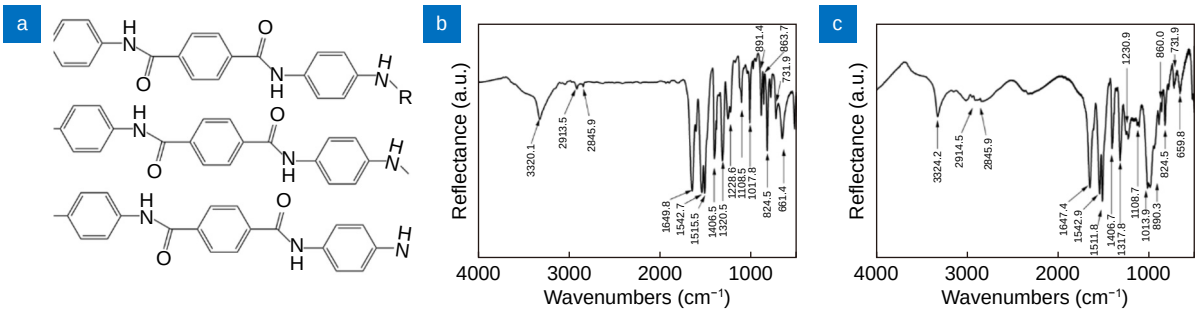

Fig. S1 | (**a**) Molecular structure of aramid. (**b**, **c**) FT-IR absorption spectra of (b) ANA and (c) PANA respectively.

Section 2: Appearance variation of JANA with different contents of Au

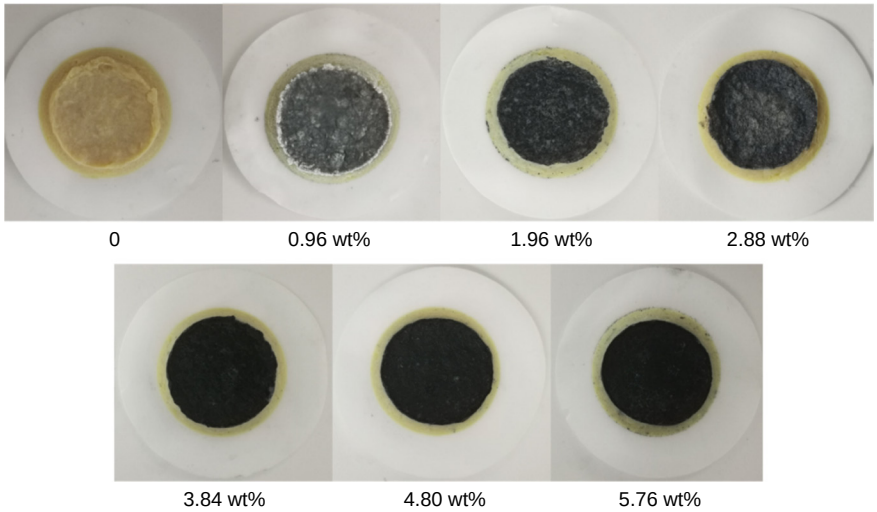

Fig. S2 | Photographs of JANA with different contents of Au nanoparticles.

Section 3: Numerical simulation of the optical absorption of JANA

To investigate the mechanism of the optical absorption by JANA, we perform full-wave simulations using 3D finite-different time-domain (FDTD) method (Lumerical software). As shown in Fig. S3(a), JANA is modelled by randomly distributed Au nanoparticles embedded in an aramid film and illuminated by a broadband plane wave source (total-field-scattered-field source). Based on the content of Au, the number of nanoparticles in 1 μm^3 aramid film is set as 27. The diameters of all the particles are equal to 43 nm. The refractive index of Au is obtained from Johnson and Christy' s

result[S2]. The refractive index of aramid is measured using an ellipsometer, as shown in Fig. S3(b). The source band ranges from 300 nm to 2100 nm. Two monitors are used to record the reflection (R) and transmission (T) within the operational band from 400 nm to 2000 nm. Absorption (A) is then calculated according to the relation that A + R + T = 1. All the boundaries of the simulated space are set as perfectly matched layers.

Figure S3(c) shows the three simulated spectra of JANA with 0.9 μm thickness. Within the entire band, R is always near zero featuring the anti-reflection effect. It is caused by the low refractive index of Au-aramid composite, which makes the effective impedance highly comparable to that of air. In this case, A is dominated by T. JANA performs high A and low T at short wavelengths, but low A and high T at long wavelengths. Short-wave absorption is mainly generated from the localized surface plasmon resonances of Au nanoparticles. Light energy can be effectively concentrated around the nanoparticles and dissipated by the oscillation of surface plasmon. Long-wave absorption is mainly generated by intrinsic extinction coefficients of Au and aramid, i.e. non-resonant decay. It is lower in absorbance than plasmonic resonances. Notably, the simulation is not in consideration of the contribution of the porous morphology of the JANA network to the optical absorption. For anti-reflection effect, porous morphology can further decrease the value and gradient of surface impedance; for non-resonant decay, the porous morphology permits light to be repeatedly reflected or scattered by the Au nanoparticles, creating longer light paths and thus higher decay intensity. Accordingly, the absorption mechanism can be briefly concluded as i) anti-reflection effect, ii) surface plasmon resonances, iii) non-resonant decay, and iv) porous effect[S3].

Figure S3(d) shows the absorption spectra of JANA with increasing thickness. Within the entire operational band, the absorbance keeps rising with the increment of the thickness. When the thickness is 18.5 μm, absorbance at any wavelength reach close to 100%. Namely, the theoretical minimum thickness for near-perfect absorption is 18.5 μm.

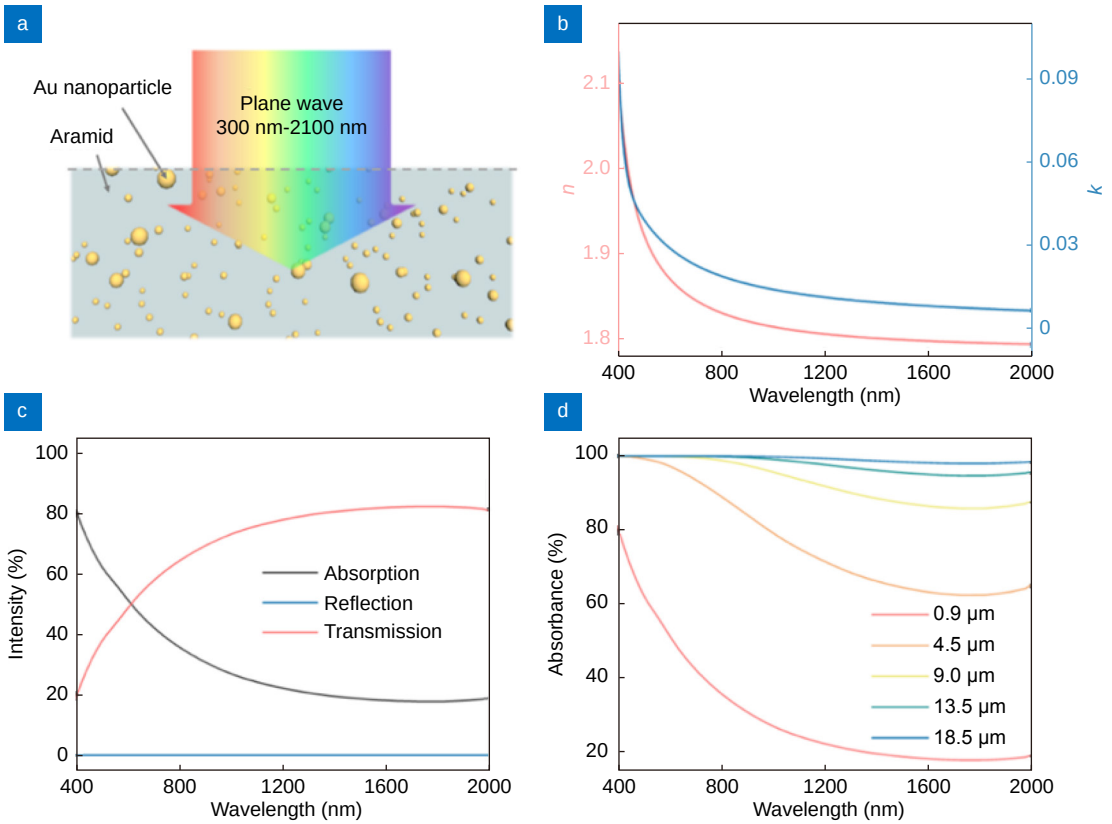

Fig. S3 | (**a**) Schematic illustration of the FDTD modeling regime. (**b**) Real and imaginary parts of the refractive index of aramid. (**c**) Absorption, reflection and transmission spectra of JANA film with a thickness of 0.9 μm. (**d**) Absorption spectra of JANA with different thicknesses.

Section 4: Wettability of aramid

To characterize the chemical wettability of aramid free from the influence of the porous morphology, we fabricate a

dense and smooth aramid film. Contact angle analysis is carried out by dropping 10 μL water on the film. As shown in Fig. S4, the two contact angles are respectively equal to 44.76°and 48.82°. We thus take the average value of 47° to describe the chemical wettability of aramid, which is apparently hydrophilic.

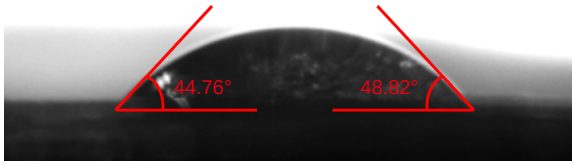

Fig. S4 | Photograph of a droplet of 10 μL water located on a dense aramid film.

Section 5: Practical ISSG process using JANA

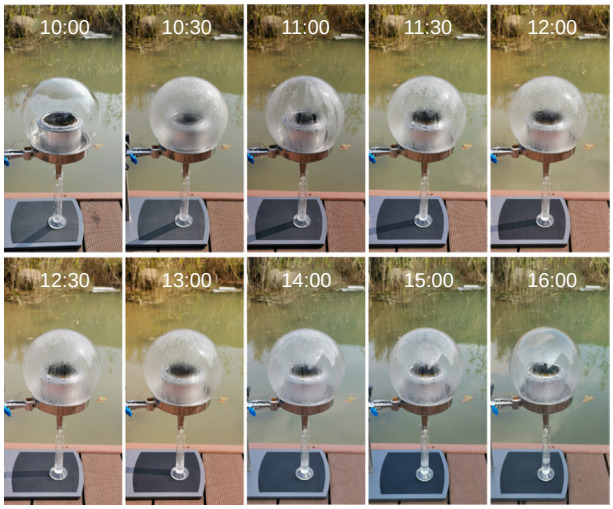

Fig. S5 | Photographs of a purification setup at different moments during a practical ISSG process.

Section 6: Quality inspection report of municipal sewage and purified water

We conduct practical purification of municipal sewage by using a homebuilt ISSG setup loaded with JANA. Figure S6 shows two water samples. Sample A is the purified water after ISSG. Sample B is the sewage sample collected from a sewer in Nanjing, China. The two samples are delivered to a water quality inspection agency. Figure S7 and S8 are the quality inspection report, in which sample A and B are in accordance with the two samples denoted in Fig. S6.

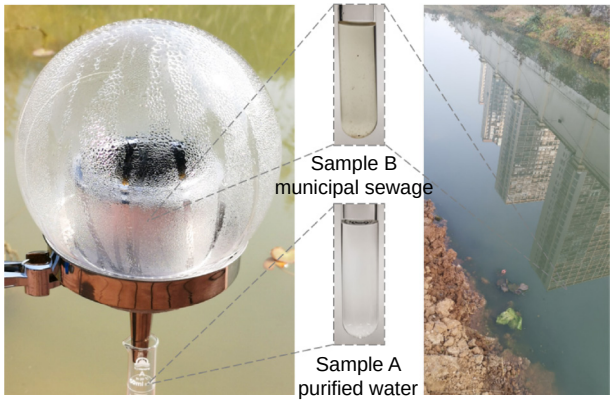

Fig. S6 | Photographs of water samples for quality inspection. Sample A is purified water produced after the ISSG process; sample B is municipal sewage collected from a sewer and put into the ISSG setup.

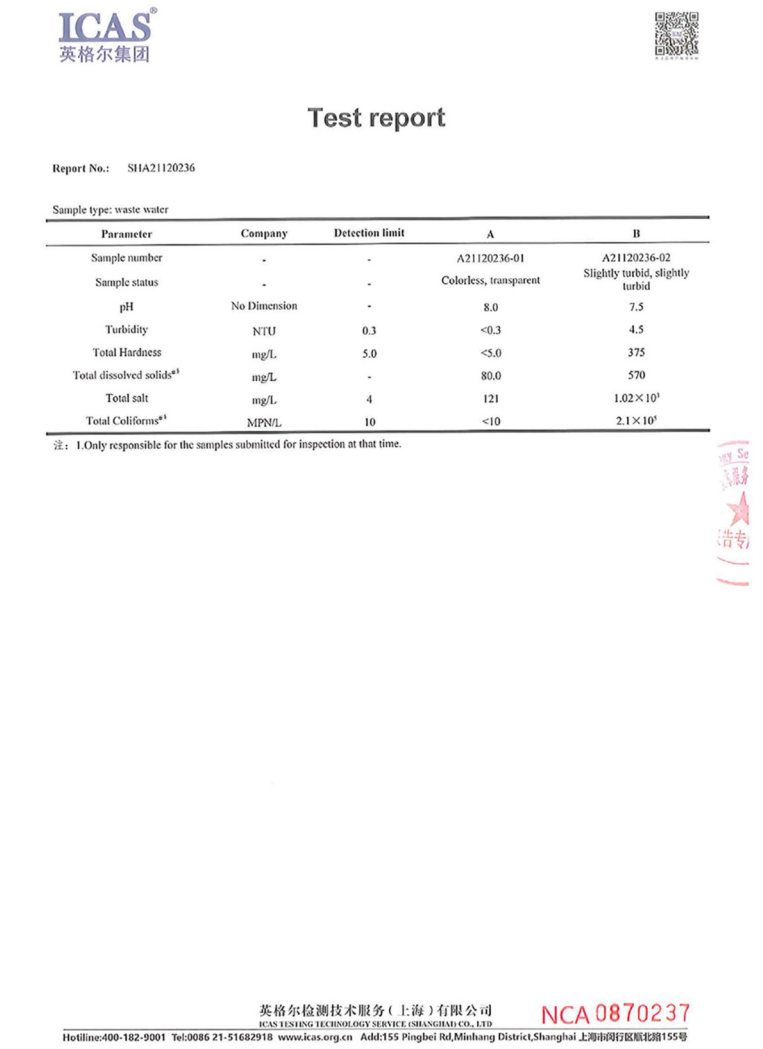

ICAS 英格尔集团

Test report

Report No.: SHA21120236

Sample type: waste water

Parameter	Company	Detection limit	A	B
Sample number	-	-	A21120236-01	A21120236-02
Sample status	-	-	Colorless, transparent	Slightly turbid, slightly turbid
pH	No Dimension	-	8.0	7.5
Turbidity	NTU	0.3	<0.3	4.5
Total Hardness	mg/L	5.0	<5.0	375
Total dissolved solids*1	mg/L	-	80.0	570
Total salt	mg/L	4	121	1.02×10^3
Total Coliforms*1	MPN/L	10	<10	2.1×10^5

注：1.Only responsible for the samples submitted for inspection at that time.

英格尔检测技术服务（上海）有限公司 NCA 0870237
ICAS TESTING TECHNOLOGY SERVICE (SHANGHAI) CO., LTD
Hotline:400-182-9001 Tel:0086 21-51682918 www.icas.org.cn Add:155 Pingbei Rd,Minhang District,Shanghai 上海市闵行区顺北路155号

Fig. S7 | Page 1 of the quality inspection report.

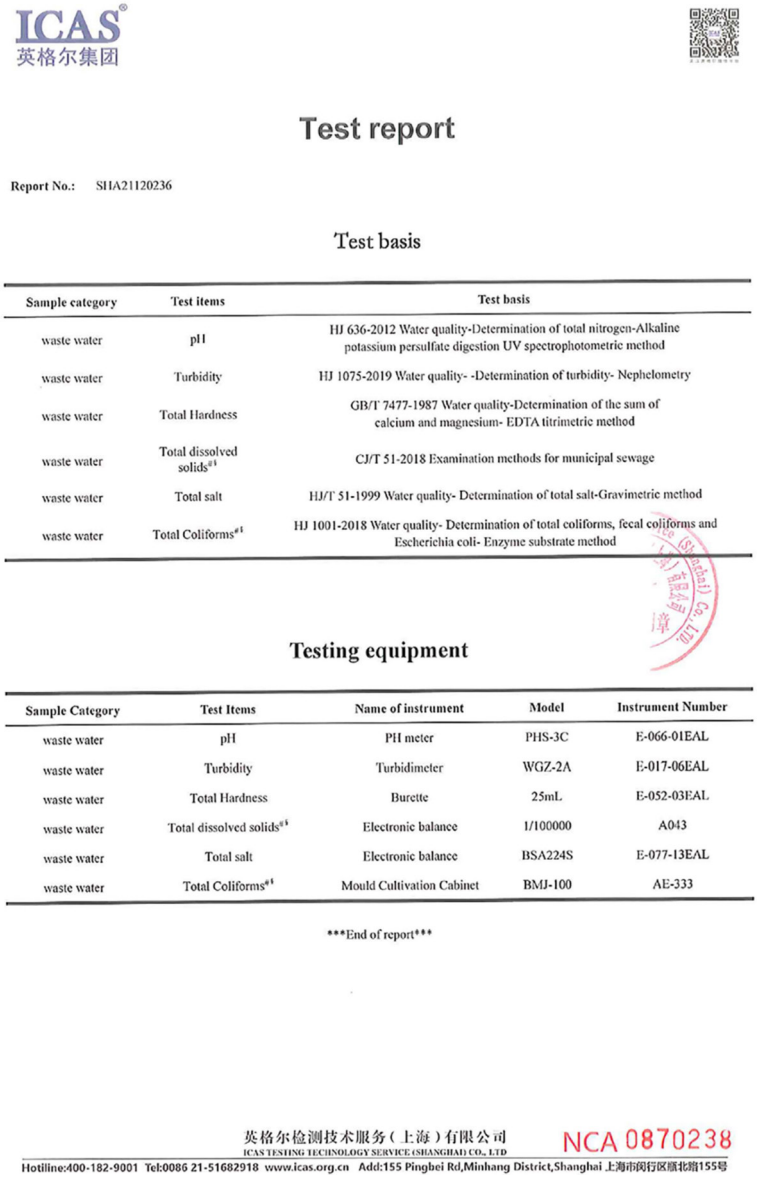

ICAS 英格尔集团

Test report

Report No.: SHA21120236

Test basis

Sample category	Test items	Test basis
waste water	pH	HJ 636-2012 Water quality-Determination of total nitrogen-Alkaline potassium persulfate digestion UV spectrophotometric method
waste water	Turbidity	HJ 1075-2019 Water quality- -Determination of turbidity- Nephelometry
waste water	Total Hardness	GB/T 7477-1987 Water quality-Determination of the sum of calcium and magnesium- EDTA titrimetric method
waste water	Total dissolved solids#§	CJ/T 51-2018 Examination methods for municipal sewage
waste water	Total salt	HJ/T 51-1999 Water quality- Determination of total salt-Gravimetric method
waste water	Total Coliforms#§	HJ 1001-2018 Water quality- Determination of total coliforms, fecal coliforms and Escherichia coli- Enzyme substrate method

Testing equipment

Sample Category	Test Items	Name of instrument	Model	Instrument Number
waste water	pH	PH meter	PHS-3C	E-066-01EAL
waste water	Turbidity	Turbidimeter	WGZ-2A	E-017-06EAL
waste water	Total Hardness	Burette	25mL	E-052-03EAL
waste water	Total dissolved solids#§	Electronic balance	1/100000	A043
waste water	Total salt	Electronic balance	BSA224S	E-077-13EAL
waste water	Total Coliforms#§	Mould Cultivation Cabinet	BMJ-100	AE-333

End of report

英格尔检测技术服务（上海）有限公司 NCA 0870238
ICAS TESTING TECHNOLOGY SERVICE (SHANGHAI) CO., LTD
Hotline:400-182-9001 Tel:0086 21-51682918 www.icas.org.cn Add:155 Pinghei Rd,Minhang District,Shanghai 上海市闵行区颛北路155号

Fig. S8 | Page 2 of the quality inspection report.

References

S1. Cao K Q, Siepermann C P, Yang M, Waas A M, Kotov N A et al. Reactive aramid nanostructures as high-performance polymeric building blocks for advanced composites. *Adv Funct Mater* **23**, 2072–2080 (2013).

S2. Johnson P B, Christy R W. Optical constants of the noble metals. *Phys Rev B* **6**, 4370–4379 (1972).

S3. Feng L, Huo P C, Liang Y Z, Xu T. Photonic metamaterial absorbers: morphology engineering and interdisciplinary applications. *Adv Mater* **32**, 1903787 (2020).